# PRESSURE DROP AND HEAT TRANSFER IN THE SODIUM TO AIR HEAT EXCHANGER TUBE BANKS ON ADVANCED SODIUM-COOLED FAST REACTOR

H. Kang<sup>1</sup>, J. Eoh<sup>2</sup>, J. Cha<sup>2</sup> and S. Kim<sup>2</sup>

<sup>1</sup> Kunsan National University, Gunsan, South Korea <sup>2</sup> Korea Atomic Energy Research Institute, Daejeon, South Korea hckang@kunsan.ac.kr, jheoh@kaeri.re.kr, jecha@kaeri.re.kr, sokim@kaeri.re.kr

#### **Abstract**

A numerical study was performed to investigate the thermal and hydraulic characteristics and build up design model of the AHX (sodium-to-air heat exchanger) unit of a sodium-cooled fast reactor. Helical-coiled tube banks in the AHX were modeled as porous media and simulated heat and momentum transfer. Two-dimensional flow characteristic appeared at the most region of AHX annulus. Pressure drop and heat transfer coefficient for rectangular, parallelogram and staggered tube banks as the main components of the AHX were evaluated and compared with Zhukauskas empirical correlations.

#### 1. Introduction

The conceptual design of the sodium-cooled fast reactor, KALIMER (Korea Advanced LIquid MEtal Reactor) has been developed, and various advanced design concepts have been continuously proposed and evaluated to satisfy the Generation IV (Gen IV) technology goals. [Hahn et al. (2007)] On the basis of a stepwise technology development, the Gen IV SFR (hereafter called advanced SFR) system is currently being developed, and its rated power was increased from the conventional 600 MWe to 1,200 MWe to improve plant economics. The design of the advanced SFR system is totally based on a maximum of passive safety features as far as it is technically feasible and economically beneficial. The IRACS (Intermediate Reactor Auxiliary Cooling System) is normally operated in a forced flow condition, while the PDRC (Passive Decay heat Removal Circuit) system relies exclusively on a natural convection heat transfer, i.e. natural circulation on the sodium-side and natural draft on the air-side. Hence independent and diverse decay heat removal (DHR) systems such as PDRC and IRACS have been employed to provide a highly reliable heat removal function from the primary heat transport system to the atmosphere during both scheduled and emergency. Two kinds of DHR systems are proposed which have different heat exchanging components and functional diversity to avoid common mode failures and to achieve a high reliability target of 10<sup>-7</sup> failure per demand. [Kim et al. (2008)] One of the most important components for the design of both DHR systems is the sodium-to-air heat exchanger (hereafter called AHX). This is because the convection resistance of the AHX shell-side air flow path is the dominant factor for determining the overall heat removal performance from the reactor core to the atmosphere, i.e. final heat sink. Hence, sufficient design considerations for the AHX to reasonably predict the pressure drop and heat transfer coefficient from the sodium tube to the air flow are required to enhance the reliability of the DHR system design.

Zhukauskas et al. (1968) greatly contributed to the thermal and flow resistance design on the circular tube banks related to the present work. They provided the experimental data for the

Reynolds and and landtl numbers. Some research on the nodified tube banks has been conducted, however their work is limited in comparison to byen, the range of the present work. It is not research on the nodified tube banks has been conducted, however their work is limited in comparison to byen, the range of the present range of tube bank arrangements.

Mittal and Bala andar (1997) conducted a numerical simulation flow past linder at low Re < 10<sup>3</sup>. Ku (2005) and Raza<del>vi et at</del>. (2008, also reported dra Lefficients for a cylinder at a low Reynold number. Several number a smulations have b performed to linder due to the complexity of the flow. applied a 3D large eddy nulation with aged Navier–Stokes eq wall model as well as an u on using the standard high Reynolds in the standa littal (2005) performed ail studies for UIS  $100 < \text{Re} < 1 \times 10^7 \text{ using a 2D}$ I. (2009) presented tim veraged drag coefficients for 0.5x10<sup>6</sup> < Ressure distribution for ₹1x10<sup>6</sup> using flow across a URANS with a standard high ε model. Many wer≝a circular cylinder have been pe umerical model comparing the empirical mmmmmm n (1977), wnitaker 1075 correlations of Hilpert (1933). 

Heat exchangers of many sur approached using one or two one equation model assumes that the same temperature, or local thermal equilibrium, using one equation for the solid and fluid phase temperature. The two-equation model includes an equation for each phase, treating the solid and fluid phase separately. Due to the configuration of the lad wave equation model, Raviany (1983), Vafafafand Kim (1989) and Haji-Sheikh et al. (2006) used the one equation model in analyzing convection heat transfer in porous media.

In this study, fundamental features of the pressure drop and heat transfer performance of the air flow system across tube banks of the AHX were investigated by using a multi-dimensional CFD analysis. The numerical methods regarding the pressure drop and heat transfer calculations for this type of air flow system were also evaluated by comparing conventional correlations after checking the effectiveness of the numerical methods for the flow across a cylinder. Based on the evaluation results, design guides for a the reliable and safe heat transfer performance of the AHX with helical-coiled tube banks are recommended, and specific design directions for the tube arrangement to avoid a local flow separation effect around the tube and AHX annulus are also discussed.

## 2. System description of the advanced SFR

The heat transport system of the advanced SFR was designed to be a pool-type system to enhance system safety through slow system transients, where primary sodium is contained in a reactor vessel. The heat transport system is composed of a primary heat transport system (PHTS), an intermediate heat transport system (IHTS), a steam generating system (SGS) and a residual heat removal system (RHRS) as shown in **Figure 1**. During normal power operation mode, heat generated from the reactor core is transferred to the SG through the PHTS and IHTS via Intermediate Heat Exchangers (IHXs) as shown in **Figure 2**.

With regard to the design of the AHX, its component diversity is mainly achieved by two different designs of the heat exchanging tube bundle, which are helical-coil type and compensated straight tube type. In the PDRC design, the AHX has drum type tube bundles with a total of ten cylindrical rows of un-finned tubes, a central inlet header arranged at the top of the tube bundle with a separated expansion vessel for the PDRC sodium loop, and an outlet common header below the tube bundle. The FDHX (forced-draft sodium-to-air heat exchanger) for the active IRACS system consists of four pass serpentine tube bundles with an inclined tube arrangement, and the shell-side air flow is assumed as a cross flow across the tube bank. The tube bank is attached to an upper inlet and a lower outlet header. The headers and tube bundle are mounted in a support structure that provides support for the tubes allowing for thermal expansion. Functional diversity can also be achieved by different operating conditions of the two groups of AHXs during standby condition in the reactor power operation mode. Consequently, different air-cooling mechanism of the AHXs and FDHXs induce different heat losses and cool-down performance in the AHX and FDHX.

Table 1 Geometry and operation conditions of AHX (sodium-to-air heat exchanger) used in the present work

VI.	ie present work		
Parameter	Symbol	Unit	Data
Heat capacity	Q	MW	8.112
Pressure drop of AHX annulus	$\Delta P$	kPa	190
Frontal velocity	u	m/s	6.1
Inlet temperature of air	$T_{in}$	K	313.15
Outlet temperature of air	$T_{ex}$	K	551.18
Inlet temperature of sodium	$T_{s,in}$	K	776.31
Outlet temperature of sodium	$T_{s,ex}$	K	623.07
Height of annulus	Н	m	5.91
Outer radius of annulus	$r_o$	m	1.835
Inner radius of annulus	$\mathcal{F}_i$	m	1.0
Tube diameter	D	m	0.054
Longitudinal tube pitch	$S_{\scriptscriptstyle L}$	m	0.054
Transverse tube pitch	$S_T$	m	0.054
Interior angle of tube bank	$\theta$	deg	90, 79.5
Number of tube row	$N_r$	1	71.6
Number of tube step	$N_s$	-	10
Volume of annulus	$V_{core}$	m <sup>3</sup>	43.95
Surface area of annulus	$A_{core}$	$m^2$	105.3
Hydraulic diameter of annulus	$D_{h,core} (= 4V_{core} / A_{core})$	m	1.67
Number of tubes	$N_{t}$	-	196
Total length of tubes	$L_{t}$	m	6429.5
Surface area of tubes	$A_{\iota}$	$m^2$	1090.7

Hydraulic diameter of tube	$D_{h,t}(=4V_{air}/A_t)$	m	0.1072
Compactness	$A_{t}$ / $V_{core}$	$m^2/m^3$	24.82
Porosity	$\alpha$	-	0.66
Permeability	K	$m^2$	$3.63 \times 10^{-6}$
Quadratic resistance coefficient	eta	kg/m <sup>4</sup>	0.864

### 3. Numerical Simulation Method

**Figure 2 and Table 1** are the configuration of tube banks and typical operation conditions in the AHX annulus of the present study. The tube banks are consisted of a total of ten steps (radial direction of AHX annulus, r direction of **Figure 2 (a)**) and on average of 71.6 rows (vertical direction of AHX annulus, y direction of **Figure 2 (a)**) as shown in **Figure 3 (a)**. The reference configuration is the parallelogram tube banks ( $\theta = 79.5^{\circ}$ ) as shown in **Figure 3 (b)**, and it is compared with the rectangle ( $\theta = 90^{\circ}$ ) and staggered tube banks as shown in **Figure 3 (c)**.

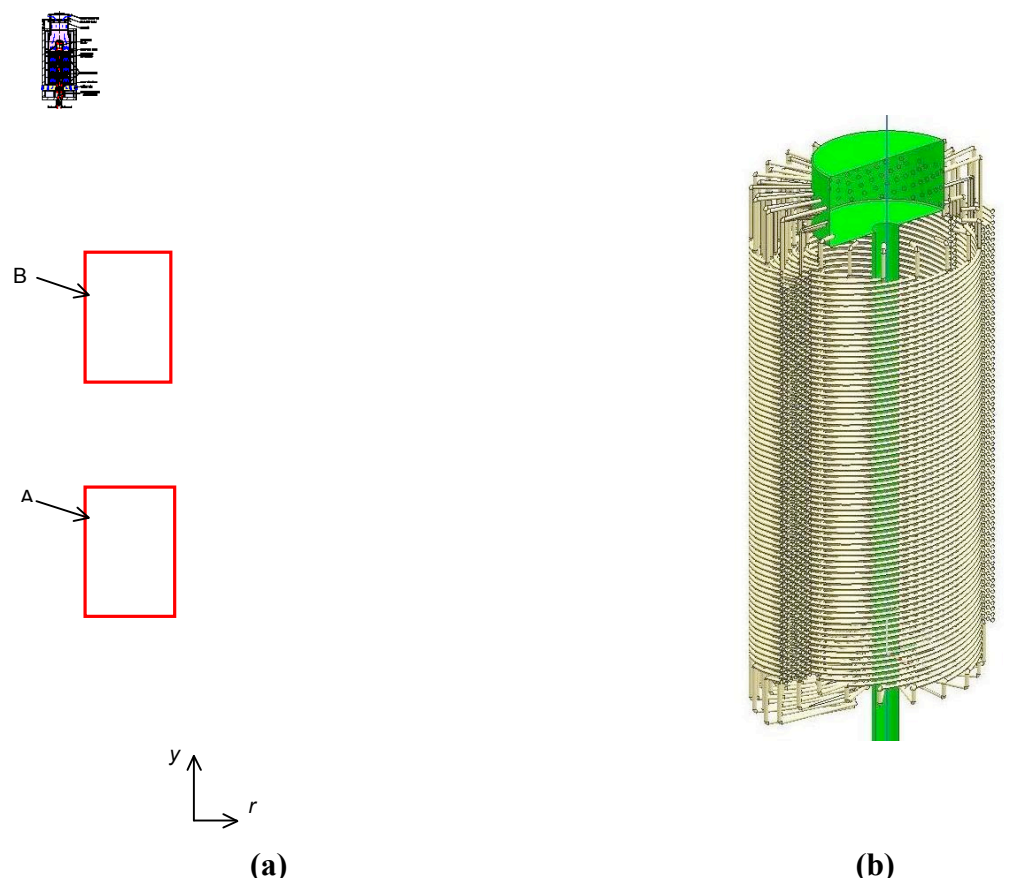


Figure 2 Schematics of the AHXs (sodium-to-air heat exchangers) (a) cross view, (b) tube bank annulus.

The heat transfer coefficient of the tube banks can be obtained as follows.

$$Nu_{D} = \frac{hD}{k} = C_{1}C_{2} \operatorname{Re}_{D}^{m} \operatorname{Pr}^{0.36} \left(\frac{\operatorname{Pr}}{\operatorname{Pr}_{s}}\right)^{1/4}$$
 (1)

$$1000 < \text{Re}_D < 2 \times 10^6, 0.7 < \text{Pr} < 500$$
 (2)

The coefficient  $C_1$ ,  $C_2$  and m are the correction factor and exponent of Re number for the number of tube rows and the alignment of tube bank respectively. The properties are defined at the film temperature, and the  $Pr_s$  means the Prandtl number at tube wall temperature. The Reynolds number is based on the maximum flow velocity,  $V_{\rm max}$  at the minimum cross section.

$$Re_D = \frac{\rho V_{\text{max}} D}{\mu} \tag{3}$$

The pressure drop across the tube bank can be expressed as below.

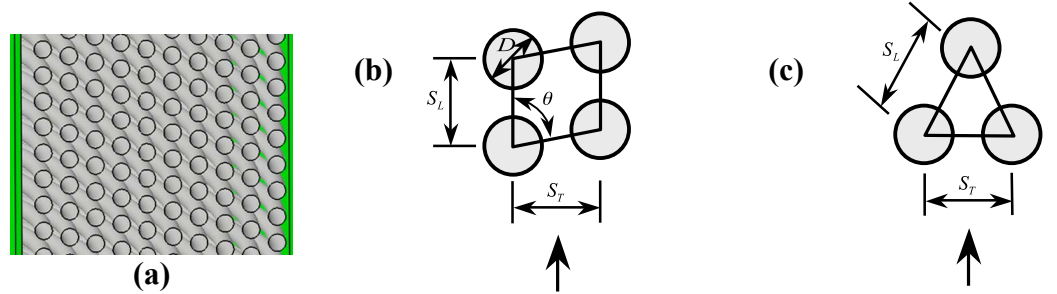


Figure 3 Tube bank (a) cross view of the present AHX, (b) rectangle and parallelogram (c) staggered tube banks.

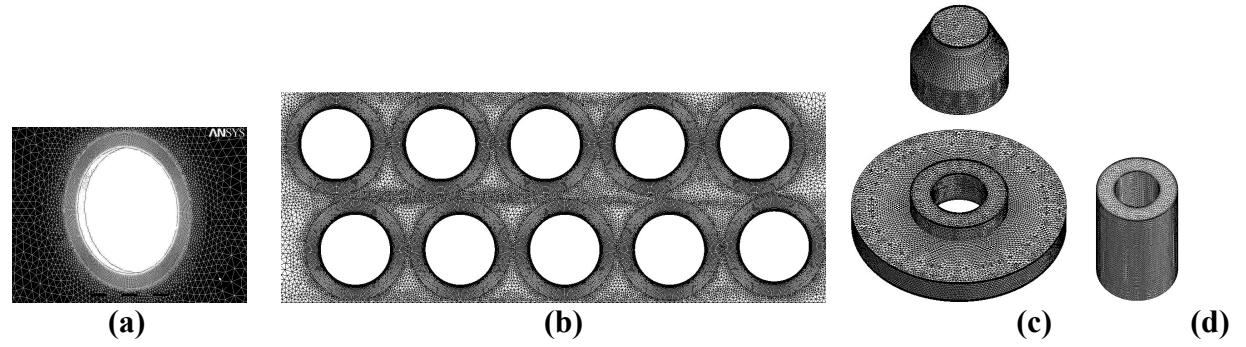


Figure 4 Grids used in the present numerical simulation (a) flow across a cylinder across, (b) flow trough the tube banks, (c) inlet and outlet of the AHX, (d) AHX annulus.

$$\Delta P = N_L \chi f \left( \rho V_{\text{max}}^2 / 2 \right) \tag{4}$$

Where  $N_L$ ,  $\chi$  and f are the number of tube rows, correction and friction coefficient respectively. The correction coefficient can be obtained from the table as a function of the number of tube rows and the tube bank alignment.

The AHX is made up of multiple tube banks. Sodium flows from the upper to the lower storage tanks. Air flows into the lower part, is heated and exhausts at the upper part. The heat transfer mechanism of the airside and tubes inside of the AHX is the natural convection from the viewpoint of the AHX system while the forced convection is from the viewpoint of the tube banks.

The CFX 10 (2006) was used in the present simulation. The preliminary numerical simulation was performed to search for the best simulation conditions for the flow across a cylinder under the operating conditions. After comparing the empirical correlations of heat transfer and pressure drop with numerical results, the best turbulent model was the  $k - \omega$  SST. The number of surface elements was increased to 6.21 x 10<sup>5</sup>, attaining an asymptotically converging value that agreed reasonably with the experimental data. The first grid near the wall was  $y^+ \sim 1$  to apply the law of wall. **Figure 4 (a)** and **(b)** show grids in the present numerical simulation of a single tube and tube bank respectively.

The AHX was classified as the inlet and outlet parts without tube bank and the AHX annulus with tube bank. The AHX annulus was approximated as the porous media because of its geometric complexity. Porosity is the ratio of air to total volume,  $\alpha = 1 - V_t / V_{core}$ , is 0.66. Permeability is part of the proportionality constant in Darcy's law that relates the discharge (flow rate) and fluid physical properties (e.g. viscosity), to a pressure gradient applied to the porous media. The permeability and volumetric heat generation was defined as below.

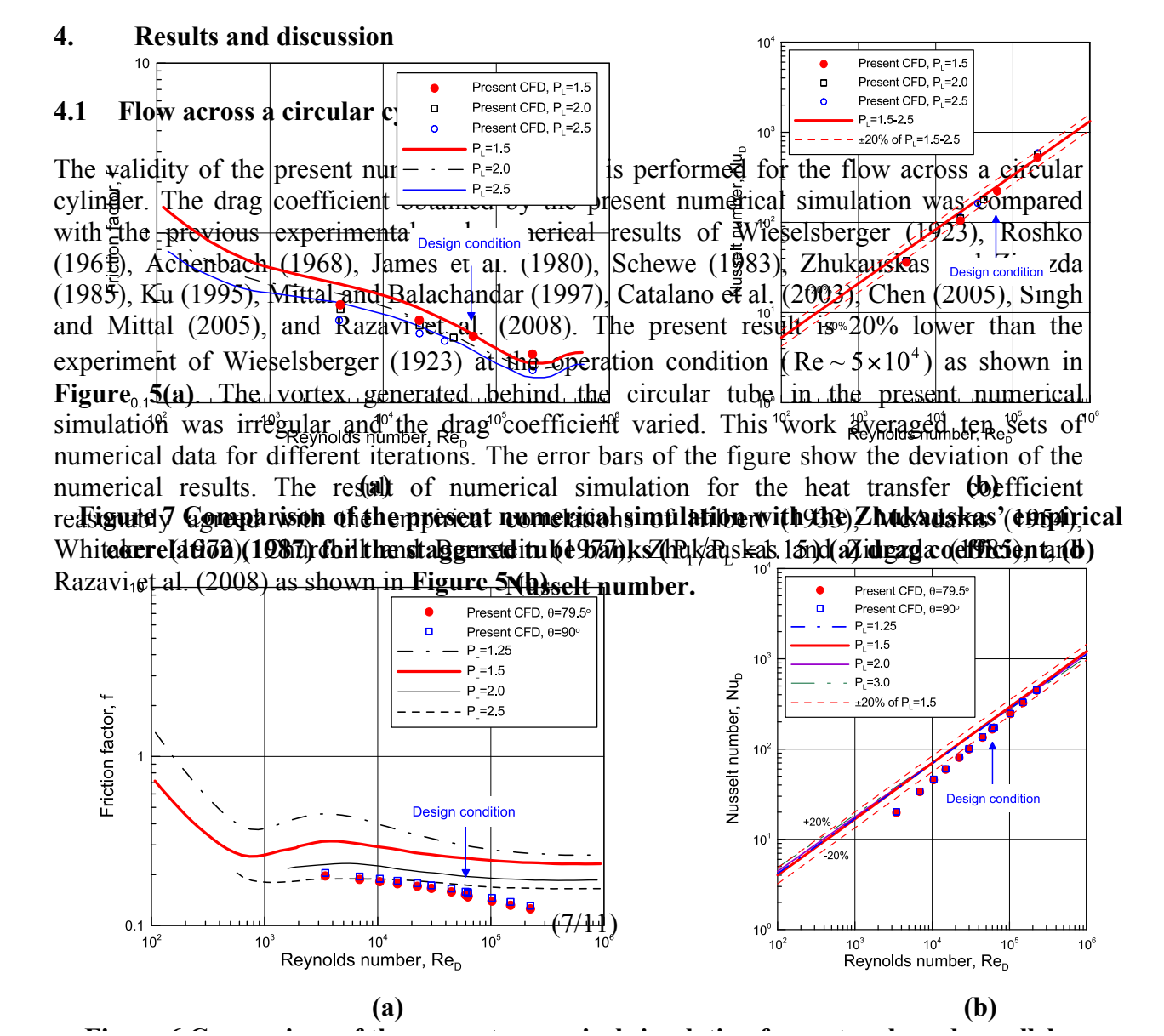
$$\hat{u} = -\frac{K}{\mu} \frac{\partial P}{\partial v} \tag{5}$$

$$\dot{q} = \frac{\dot{m}c_p \left(T_{ex} - T_{in}\right)}{V_t} \tag{6}$$

$$\beta = \frac{\mu}{\hat{u}K} \tag{7}$$

The  $\frac{\partial P}{\partial v}$  and  $\mu$  are the pressure gradient in the flow direction and directi the fluid respectively. The term  $\bar{u}$  respectively and is defined as the volumetric flow rate over the total area. The coefficient K is the permeability-and is independent of nature of the fluid but depends on  $C_{and bet}^{Captaget}$  of the medium. The parameter  $\beta$  the quadratic resistance coefficient sign and Mittal 2005 CFX. The values used in the present study are listed in the **Table 1**. The surface mesh of this simulation is as shown in **Figure 4**(c) and (d). The standard k- is subject to model was used because the Reynolds number based on the AHX annulus of the present numerical simulation were 10<sup>-5</sup> for the sum of residuals and 0.1% for the conservation balances of the conservation equations. Chen(2005) Razavi & Farhangmehr(2008) 10 10 10<sup>3</sup> Re<sub>D</sub> Re<sub>D</sub> **(b)** (a)

Figure 5 Comparison of the present numerical simulation with the previous works for the forced convection on a single tube (a) drag coefficient, (b) Nusselt number.



## 4.2 Pressure drop and heat transfer of tube banks

**Figure 6** compared the numerical result of the drag coefficient and Nusselt number for the parallelogram tube banks with Zhukauskas' experimental correlation (1968) for  $P_T = S_T/D = 1.5$  and  $P_T/P_L = 1.0$ . The pressure drop and heat transfer coefficient of the rectangular tube banks and parallelogram tube banks were within 2~3%. Both pressure drop and heat transfer of the rectangular tube banks were greater than those of the parallelogram tube banks. This is because the minimum cross-section area of the rectangular tube banks for the flow is smaller than parallelogram tube banks. However the present numerical simulation underestimated the pressure drop by about 40% less than Zhukauskas' empirical correlation for the rectangular tube banks. The Nusselt number was also underestimated and showed bigger deviation in the low Reynolds number range. The reason is that the vortexes behind the tubes are isolated from the airflow between the tubes. The airflow between the tubes is restricted to meet the new heat transfer surface. The tube arrangement should be taken care of in the design of the AHX.

**Figure 7** compares the pressure drop and heat transfer results obtained by the numerical simulation on the staggered tube banks with Zhukauskas' correlation for  $P_T/P_L = 1.15$ . The trend of the results was similar to those of the rectangular tube banks. However the deviation between the empirical correlation and numerical simulation of the staggered tube banks was smaller than those of the rectangular tube banks. The effect of the longitudinal tube pitch ratio  $(P_L = S_L/D)$  was small in the staggered tube banks. The Nusselt number of the numerical simulation agreed with the correlation within 20%.

## 4.3 Thermal and hydraulic characteristic of AHX

The uniformity of the airflow inside tube bank is important in the heat transfer performance of the AHX. The AHX inlet and outlet shapes of **Figure 2 (a)** 'A' and 'B' influence the uniformity of the flow. In the present work, the heat transfer of the rectangular edge, 45° chamber and shape of the curved side were reviewed and compared. The surface area density of the AHX tube bank is high, and it approximated as porous media. The inlet of the AHX is a perpendicular corner, where a strong vortex is generated right behind the perpendicular corner. A vortex is also formed behind the perpendicular edge of the outlet. In the case of the inlet with the 45° chamber and round shape, the size of the vortex at the inlet significantly decreases and air flows smoothly along the shapes. It can be found that the 1:2 inclination chamber significantly mitigates the vortex to the perpendicular corner at the outlet.

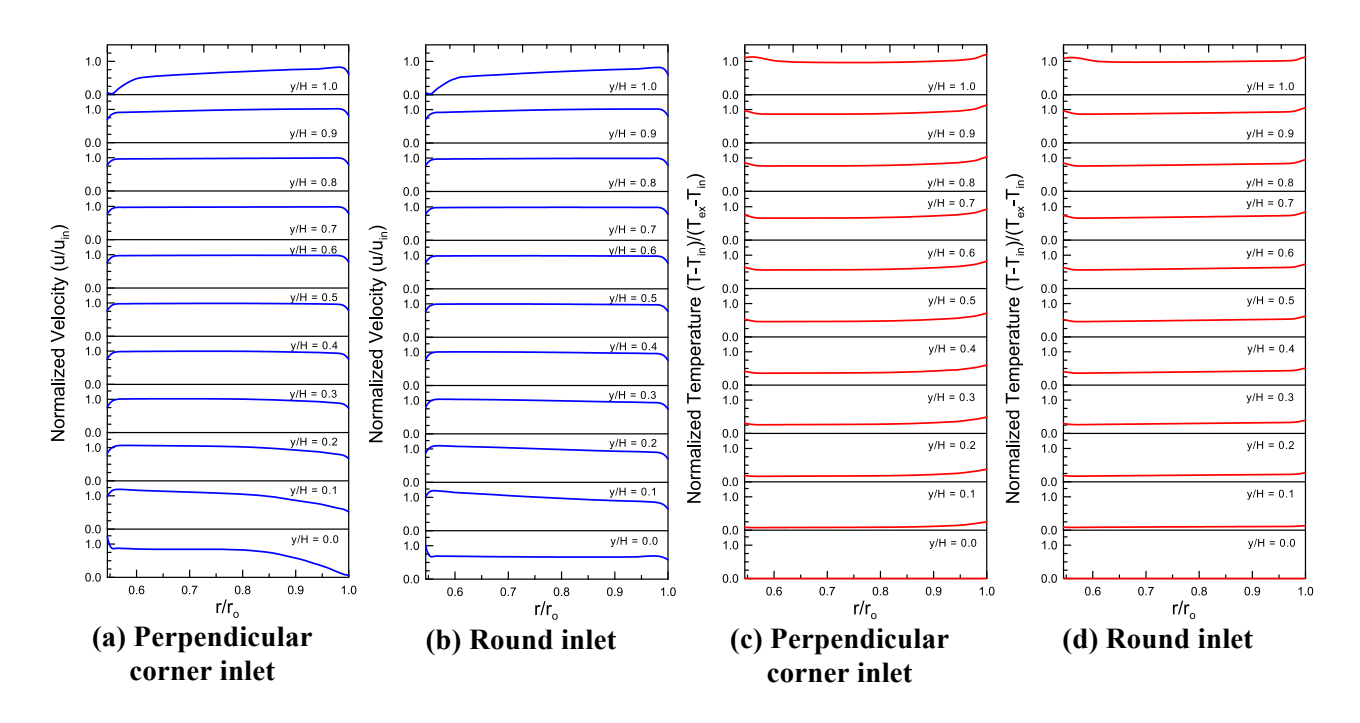


Figure 8 Velocity distribution of air at the AHX for the perpendicular corner inlet configuration.

**Figure 8 (a)** and **(c)** show the velocity and temperature distributions along the radial direction r for 10 sections in vertical direction y of the AHX annulus for the perpendicular corner shape. The velocity and temperature were normalized to the inlet velocity and inlet/outlet temperatures respectively. At the bottom part (y/H < 0.3), the air velocity is higher in the AHX annulus inside than the outside, while the air temperature is higher in the AHX annulus outside than the inside. This is because the inlet airflow is driven to the bottom of the AHX inner wall from the outside. The velocity distribution changes, in the inlet region, 0 < y/H < 0.3, and the entrance effect exists. The velocity is the same as the inlet velocity within 5% in the region 0.22 < y/H < 0.95. Therefore, it can be treated as a two-dimensional flow in the region. The temperature distribution was almost linear along the flow direction. **Figure 8 (b)** and **(d)** show the velocity and temperature distributions when the inlet shapes of the AHX are round. The distributions of the perpendicular corner in 0 < y/H < 0.3 are improved to a two-dimensional flow. If the inlet shape of the AHX is designed as the shape proposed in the present work, the thermal load of the AHX will be more uniformly distributed and the safety of the AHX would be improved.

### 5. Conclusions

As a result of performing a numerical simulation for the heat flow characteristic of the AHX (sodium-to-air heat exchanger) and tube banks that are the main cooling devices of a sodium cooled reactor, the following conclusions were reached in this study:

When the AHX to the tube banks of five rows were simplified and compared, the parallelogram tube banks having 79.5° in the present design of the AHX showed similar thermal and hydraulic characteristics to the rectangular tube banks that have 90°.

The pressure drop and heat transfer of the staggered tube banks were higher than the parallelogram tube banks by 80% and 40% respectively. The pressure drop prediction for the parallelogram and staggered tube banks were lower than Zhukauskas' correlation by 40% and 25% respectively and the heat transfer coefficients were within 20% of the correlations.

When the AHX was modelled as porous media and an approximate calculation was performed, it showed two-dimensional thermal characteristics at the inlet area, 0 < y/H < 0.3. When the inlet shape was changed to a chamber and round, the size of the inlet area is reduced and the uniformity of flow was enhanced.

An empirical verification of the results of numerical simulation will be required in the future.

# 6. Acknowledgements

This work is the outcome of the nuclear R&D program (KAERI/CM-1278/2009) supported by the Ministry of Education, Science and Technology (MEST) and Manpower Development Program for Energy and Resources supported by the Ministry of Knowledge and Economy (MKE).

## 7. References

- [1] Achenbach, E., "Distribution of local pressure and skin friction around a circular cylinder in cross-flow up to Rex106", J. Fluid Mechanics 34, 1968, 625–39.
- [2] ANSYS, Inc., "ANSYS CFX Training Manual", Vol. 124, 2006.
- [3] Catalano P., et al., "Numerical simulation of the flow around a circular cylinder at high Reynolds numbers", Int. J. Heat Fluid Flow 24, 2003, 463-9.
- [4] Chen, H., et al., "A cell-centered pressure based incompressible Navier-Stokes solver", 43rd AIAA Aerospace Science Meeting and Exhibit, Reno, Nevada, USA. 2005.
- [5] Churchill, S.W. and Bernstein, M., "A correlating equation for forced convection from gases and liquids to a circular cylinder in cross flow", Transaction of the ASME 99, 1977, 300-306.
- [6] Hahn, D., et al., "KALIMER-600 Conceptual Design Report. KAERI/TR-3381/2007", Korea Atomic Energy Research Institute, 2007, Daejeon, Korea.
- [7] Haji-Sheikh, A., et al., "Heat transfer in the thermal entrance region for flow through rectangular porous passages", Int. J. Heat and Mass Transfer 49, 2006, 3004-3015.
- [8] Hilpert, R., "Wärmeabgabe von geheizten Drähten und Rohren im Luftstrom. Forschung im Ingenieurwesen", 4, 1933, 375-385.
- [9] James, W.D., Paris, S.W., Malcolm, G.V., "Study of viscous cross flow effects on circular cylinders at high Reynolds numbers" AIAA J. 18, 1980, 1066–72.

- [10] Kaviany, M., "Laminar flow through a porous channel bounded by isothermal parallel plates", Int. J. Heat and Mass Transfer 28, 1985, 851-858.
- [11] Kim Y.I., et al., "SFR deployment strategy for the re-use of spent fuel in Korea. Nuclear Engineering and Technology" 40, 2008, 517-526.
- [12] Ku, H.C., "Solution of flow in complex geometries by the pseudospectral element method", J. of Computational Physics, 117, 1995, 215-227.
- [13] McAdams, W.H., "Heat transmission. McGraw-Hill", New York, 1954, 252-262.
- [14] Mittal, R., Balachandar, S., "Inclusion of three-dimensional effects in simulations of two-dimensional bluff-body wake flows", <u>ASME Fluids Engineering Division Summer Meeting</u>, 1997, Vancouver, Canada.
- [15] Ong, M.C, et al., "Numerical simulation of flow around a smooth circular cylinder at very high Reynolds numbers", Marine Structures, 22, 2009,142-153.
- [16] Razavi, S.E., Farhangmehr, V. and Barar, F., "Impact of a splitter plate on flow and heat transfer around circular cylinder at low Reynolds number", J. of Applied Science 8, 2008, 1286-1292.
- [17] Roshko, A., "Experiments on the flow past a circular cylinder at very high Reynolds number", J. Fluid Mechanics 10, 1961, 345–356.
- [18] Schewe, G., "On the force fluctuations acting on a circular-cylinder in cross-flow from subcritical up to transcritical Reynolds numbers" J. Fluid Mechanics, 133, 1983, 265–285.
- [19] Singh S.P, Mittal S., "Flow past a cylinder: shear layer instability and drag crisis", Int. J. Numer Meth Fluids 47, 2005, 75-98.
- [20] Vafai K., Kim, S.J., "Forced convection in a channel filled with a porous medium: an exact solution", ASME J. Heat Transfer, 111, 1989, 1103-1106.
- [21] Whitaker, S., "Forced convection heat transfer correlations for flow in pipes, past flat plates, single cylinders, single spheres, and for flow in packed beds and tube bundles", AIChE J. 18, 1972, 361-371.
- [22] Wieselsberger, C., "Results of aerodynamic research at Göttingen (in German)", II Lieferung, 1923.
- [23] Zhukauskas, A. and Ziugzda, J., "Heat transfer of a cylinder in crossflow", Hemisphere Publishing Corporation, 1985, New York.
- [24] Zhukauskas, A., "Convective heat transfer in cross flow, Handbook of Single-Phase Convective Heat Transfer", Wiley, 1987, New York.